Ultrahigh-brightness 50 MeV electron beam generation from laser wakefield acceleration in a weakly nonlinear regime

Zhongtao Xiang; Changhai Yu ➡ ⑩ ; Zhiyong Qin ➡ ⑩ ; Xuhui Jiao; Jiahui Cheng; Qiaoxuan Zhou; Gatie Axi; Jianghua Jie; Ya Huang; Jintan Cai; Jiansheng Liu ➡ ⑩



Matter Radiat. Extremes 9, 035201 (2024) https://doi.org/10.1063/5.0189460





CrossMark





Ultrahigh-brightness 50 MeV electron beam generation from laser wakefield acceleration in a weakly nonlinear regime

Cite as: Matter Radiat. Extremes 9, 035201 (2024); doi: 10.1063/5.0189460 Submitted: 29 November 2023 • Accepted: 29 January 2024 • Published Online: 22 February 2024







Zhongtao Xiang, Changhai Yu,^{a)} D Zhiyong Qin,^{a)} Xuhui Jiao, Jiahui Cheng, Qiaoxuan Zhou, Gatie Axi, Jianghua Jie, Ya Huang, Jintan Cai, and Jiansheng Liu^{a)} D

AFFILIATIONS

Department of Physics, Shanghai Normal University, Shanghai 200234, China

^{a)}Authors to whom correspondence should be addressed: yuchanghai@shnu.edu.cn; phyzyqin@shnu.edu.cn; and liujs@shnu.edu.cn

ABSTRACT

We propose an efficient scheme to produce ultrahigh-brightness tens of MeV electron beams by designing a density-tailored plasma to induce a wakefield in the weakly nonlinear regime with a moderate laser energy of 120 mJ. In this scheme, the second bucket of the wakefield can have a much lower phase velocity at the steep plasma density down-ramp than the first bucket and can be exploited to implement longitudinal electron injection at a lower laser intensity, leading to the generation of bright electron beams with ultralow emittance together with low energy spread. Three-dimensional particle-in-cell simulations are carried out and demonstrate that high-quality electron beams with a peak energy of 50 MeV, ultralow emittance of ~28 nm rad, energy spread of 1%, charge of 4.4 pC, and short duration less than 5 fs can be obtained within a 1-mm-long tailored plasma density, resulting in an ultrahigh six-dimensional brightness $B_{6D,n}$ of ~2 × 10^{17} A/m²/0.1%. By changing the density parameters, tunable bright electron beams with peak energies ranging from 5 to 70 MeV, a small emittance of \leq 0.1 mm mrad, and a low energy spread at a few-percent level can be obtained. These bright MeV-class electron beams have a variety of potential applications, for example, as ultrafast electron probes for diffraction and imaging, in laboratory astrophysics, in coherent radiation source generation, and as injectors for GeV particle accelerators.

© 2024 Author(s). All article content, except where otherwise noted, is licensed under a Creative Commons Attribution (CC BY) license (http://creativecommons.org/licenses/by/4.0/). https://doi.org/10.1063/5.0189460

Plasma-based wakefield accelerators can produce high-brightness relativistic electron beams (e beams) of compact size $^{1-3}$ with an accelerating gradient of 100 GV/m, which is almost three orders of magnitude stronger than those provided by conventional radio-frequency (RF) accelerators. 4,5 Over the past decade, great progress has been made in developing laser-driven wakefield accelerators (LWFAs), in terms of both electron energy gain and e-beam quality, with the maximum energy being extended up to 10 GeV^{6,7} and the divergence and energy spread being reduced to 0.1 mrad and a per-mille level. 8,9 These high-energy bright e beams can find promising applications in medicine, 10,11 high-energy physics, 5 and photon science, 12,13 especially for developing compact free-electron lasers (FELs) 14,15 and novel light sources. $^{16-23}$ Nowadays, most interest is focused on high-energy LWFAs beyond 100 MeV, which

mainly rely on 100 TW class or even PW laser systems and are limited to a low repetition rate with current technology.

However, using a much smaller laser system with 1–10 TW to develop low-energy LWFAs for generating MeV-class e beams with femtosecond durations have now attracted increasing interest $^{24-28}$ because of the potential applications in ultrafast electron diffraction and electron probes, gamma-ray flashes, 29 and magnetic reconnection in laboratory astrophysics. 30 However, in comparison with e beams in the 100 MeV to 1 GeV energy range from a high-energy LWFA, the generated MeV-class e beams from a low-energy LWFA usually have large divergence and energy spread. On the one hand, for these TW-class laser systems driving an efficient LWFA, a high plasma density of $n_e \geq 10^{20}$ cm $^{-3}$ is required, making the dephasing length and pump depletion length very short, and usually inducing

significant laser–plasma instability to degrade the *e*-beam quality. On the other hand, the carrier-envelope-phase (CEP) effect of the few-cycle driving laser pulses ^{31,32} also becomes more important for the injection and acceleration and will greatly affect the *e*-beam stability and quality. Recently, several approaches have been reported to improve the *e*-beam qualities for few-cycle laser wakefield acceleration, such as by modifying the nozzle structure to increase the beam charge, ³³ employing circularly polarized light to reduce the divergence and mitigate CEP slip effects, ³⁴ and enhancing the beam stability with a specific density structure. ³⁵ Although some parameters of the MeV-class *e*-beam quality have been improved, the absolute energy spread (AES) and divergence are still relatively large, and these need to be optimized further to increase beam brightness.

In this work, we propose a scheme to generate high-quality e beams at around 50 MeV by trapping longitudinally low-divergence electrons in a weakly nonlinear wake driven by a TW-level laser system. Usually, for wave breaking mechanisms,³⁶ longitudinal injection provides better beam quality and stability compared with transverse injection. By designing a plasma with a steep density down-ramp, a moderately intense laser pulse with a normalized laser intensity of a = 1.3 can drive a weakly nonlinear plasma wave with several periods of buckets. Some paraxial electrons can slip backward axially to be trapped into the second wake, which undergoes a much faster decrease in phase velocity in the down-ramp region and therefore has a much lower injection threshold. It has been found that these injected electrons have a very small emittance of ~10 nm rad and a low absolute energy spread (AES) of ~50 keV, and the growth of emittance and energy spread are effectively restrained to maintain beam brightness during the subsequent acceleration process. As a result, output e beams with a peak energy in the 5-70 MeV range can be produced with a very small AES and a

minimum emittance of \sim 28 nm rad, making them suitable for practical applications in ultrafast electron diffraction, 37,38 in coherent radiation source generation, $^{39-41}$ and as injectors for GeV particle accelerators. 42

Figure 1 illustrates the overall generation of high-brightness e beams from a weakly nonlinear LWFA with a typical densitytailored plasma that has three down-slope distributions. As shown in Fig. 1(a), a steep density down-ramp, dropping from a peak density $n_p = 1.5 \times 10^{19}$ cm⁻³ at $z = 400 \ \mu \text{m}$ to $n_0 = 0.9 \times 10^{19}$ cm⁻³ within a steep down-ramp length $L_{d1} = 13.5 \mu m$, which is longer than the plasma wavelength $\lambda_p = 8.6 \ \mu \text{m}$, is introduced to manipulate the wake phase velocity of the second bucket and significantly reduce the electron velocity required for injection via the density down-ramp injection. 8,43-46 This kind of sharp density down-ramp can actually be produced by inserting a specific blade placed below a supersonic gas nozzle⁴³ or by the expansion of a pre-ionized plasma.⁴⁴ The phase velocity of the excited plasma waves⁴⁷ can be expressed as $\beta_p = [1 + (\xi/2n_e)dn_e/dz]^{-1}$, where n_e is the density of the plasma and $\xi = z - ct < 0$ is the longitudinal coordinate in the comoving frame (ξ < 0 behind the peak of the laser pulse). At the steep density down-ramp, the local phase velocity of the plasma wave, which is expressed as $\beta_{p,m} = [1 + md\lambda_p/dz]^{-1}$ with $\xi = -m\lambda_p$ (where *m* is the serial number of the wake structure behind the laser pulse, i.e., m = 2 for the second bucket), will decrease rapidly and the electrons converging into the tail of the second wake will more easily exceed the local phase velocity than the first wake to realize electron injection. To obtain insight into the whole process of electron injection, acceleration, and the evolution of the plasma wave, we have conducted three-dimensional (3D) simulations using the Fourier-Bessel particle-in-cell (FBPIC) code. 48 The simulation window is set to a size of $60 \times 40 \ \mu\text{m}^2$ with a 2400×800 grid cell along the propagation direction z and the transverse azimuthal direction

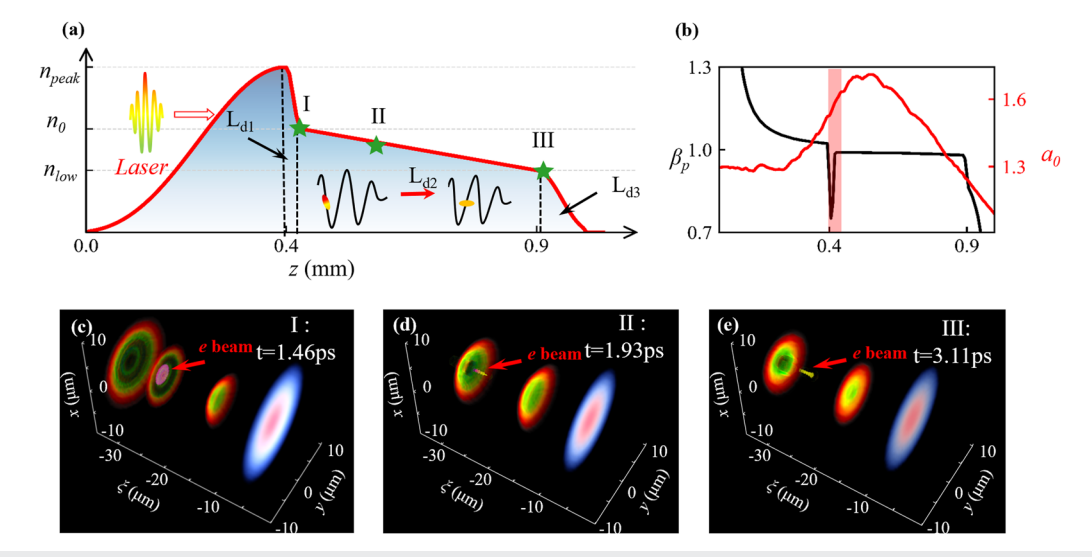


FIG. 1. (a) Schematic illustration of laser pulse propagation in a typical density-tailored plasma with three down-slope distributions, where L_{d1} , L_{d2} , and L_{d3} represent the injection stage, acceleration stage, and transportation stage, respectively. (b) Evolution of normalized laser intensity and wake phase velocity in the plasma. (c)–(e) 3D views of TW laser-driven wakefield acceleration using FBPIC simulations, for three segments at t = 1.46, 1.93, and 3.11 ps, respectively.

r, and 16 macroparticles per cell. The plasma is pre-ionized with an open boundary. A linearly polarized laser pulse of 120 mJ and with a central wavelength $\lambda_L=800$ nm enters the plasma from the left boundary into the simulation box. The laser pulse with an ontarget peak power of 8 TW has a spatiotemporal Gaussian profile with a spot radius $r_0=12~\mu{\rm m}$ and a full width at half maximum (FWHM) duration of 15 fs. The peak intensity of the input driving laser pulse is 3.6×10^{18} W/cm², corresponding to a normalized laser intensity $a_0=1.3$.

Figure 1(b) shows the evolution of the normalized laser intensity a and the phase velocity of the second wake $\beta_{p,2}$ along the propagation. The wake phase velocity $\beta_{p,2}$ decreases rapidly to 0.76 at the density down-ramp at around $z=400~\mu m$. During the propagation in the density-tailored plasma, the driving laser only self-focuses smoothly to reach its maximum normalized laser intensity of $a_{\rm max}\approx 1.6$, ensuring that a weakly nonlinear plasma wave is excited instead of a strongly nonlinear bubble. Figures 1(c)–1(e) show 3D views of the TW laser-driven wakefield acceleration from FBPIC simulations for three segments at t=1.46, 1.93, and 3.11 ps, respectively. Electrons are injected in the second wake at the density down-ramp around t=1.46 ps. Owing to the moderate laser intensity, no electrons can be trapped in the first wake.

To understand the mechanism of longitudinal electron injection in this regime, the trajectories of electrons of interest have been carefully traced and analyzed. As presented in Figs. 2(a)–2(c), since the ponderomotive force $F_p \propto \nabla a^2$ for a moderately intense laser beam is not large enough to expel all electrons transversely, a thin tabular electron sheath appears mainly at the tail of the plasma wave⁴⁹ instead of a circular bubble structure. It is observed that

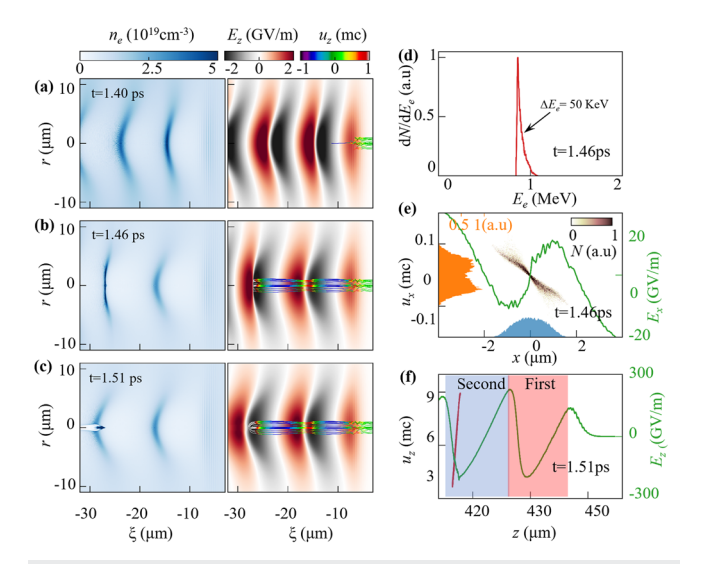


FIG. 2. (a)–(c) Plasma density, longitudinal acceleration field, and trajectory of injected electrons at different times $t=1.40,\ 1.46,\$ and 1.51 ps, respectively. (d) The e-beam energy spectrum at injection time t=1.46 ps. (e) Corresponding transverse density distribution of e-beam (blue shading), focusing field (green curve), and transverse momentum distribution (orange shading). (f) Longitudinal velocity distribution (red curve) and observed longitudinal acceleration field (green curve) of e beam at t=1.51 ps after L_{d1} .

from t = 1.40 to 1.51 ps, some backward-moving paraxial electrons with a very small transverse oscillation amplitude slip backward through the center of the first periodic wake and are directly injected into the rear of the enlarging second bucket. Before the injection, these paraxial electrons have undergone deceleration and acceleration twice during their backward movement from the first wake to the second one. Accordingly, the longitudinal momentum u_z first decreases but then increases until the electrons' longitudinal velocity is larger than the second wakefield phase velocity to realize the longitudinal injection, where the wake expansion is clearly observed at the downward density transition L_{d1} . The minimum energy for the electrons' longitudinal capture into the wake can be estimated as Ref. 50 $\gamma_{\min} \approx \beta_p/(2\Delta\phi) + \Delta\phi/(1+\beta_p)$ in the limit of $\gamma_p\Delta\phi \gg 1$, where $\gamma_p = (1 - \beta_p^2)^{-1}$ is the normalized Lorentz factor of the plasma wave and $\Delta \phi = \phi_{\rm max}^{\rm T} - \phi_{\rm min}$ is the difference in the wake potential ϕ = $e\Phi/m_ec^2$ in a single wake period. With an undifferentiated wake strength of $\Delta \phi_1 \approx \Delta \phi_2$, the electrons can be injected more easily into the second wakefield for a smaller phase velocity $\beta_{p,2} < \beta_{p,1}$ as compared with the first wake. It is found that this injected e beam has a very short duration of <5 fs, accompanied by an ultralow AES of ~50 keV, as shown in Fig. 2(d).

Apart from the ultralow AES electron injection, these longitudinally injected electrons have an ultralow emittance with only tens of nm rad. As presented in Figs. 2(e) and 3(a)–3(c), the injected e beam exhibits an ultranarrow transverse momentum distribution of $\Delta u_x\approx 0.03 m_e c$ and a very small transverse size of $\Delta x\approx 0.4~\mu m$ at $z=420~\mu m$, corresponding to a normalized emittance of 10 nm rad. It then increases to 32 nm rad at $z=450~\mu m$ and then is eventually saturated around 28 nm rad. Meanwhile, the trapped electrons undergo small betatron oscillations with a decreasing transverse size of ~0.1 μm during the following acceleration. By contrast, if the intensity of the driving laser pulse is increased to a=2.5, the plasma wave evolves into the bubble regime, where electrons are

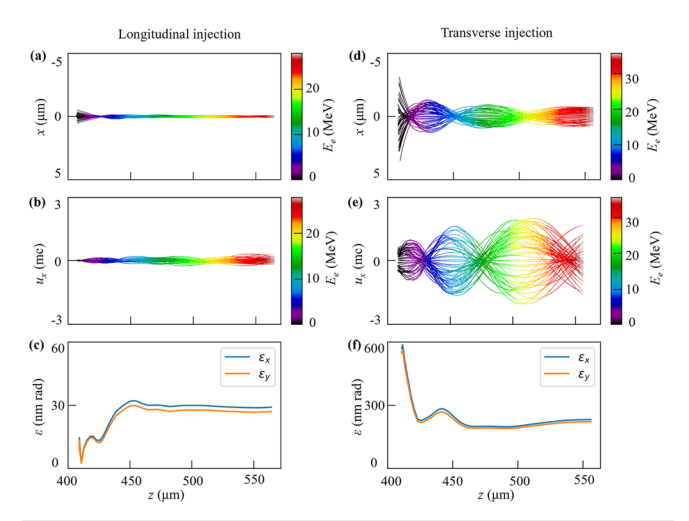


FIG. 3. Evolution of transverse position [(a) and (d)], transverse momentum [(b) and (e)], and emittance [(c) and (f)] of e beams for longitudinal injection in a weakly nonlinear LWFA [(a)–(c)], as compared with the transverse injection case for the bubble regime [(d)–(f)].

mostly expelled outward to form a circular bubble sheath, and the typical transverse injection is then induced at the tail of the wake. In this case, the transverse oscillation amplitude will increase by nearly an order of magnitude to be larger than ~1.5 μ m, and the transverse momentum u_x also increases to ~2 $m_e c$, corresponding to an emittance larger than 200 nm rad, as shown in Figs. 3(d)-3(f). It is verified that this longitudinally localized electron injection in a tailored plasma using a moderately intense driving laser favors high-brightness MeV-class e-beam generation along with ultralow emittance.

After injection, the *e* beam undergoes natural chirp self-compensation to achieve a low energy spread. As shown in Fig. 4(c), when the steep density down-ramp is terminated, the injected *e* beam has an ultralow AES of ~50 keV with a slight negative energy chirp of 0.05 MeV/ μ m, since the head of the beam was injected earlier and gained more energy than the tail. Over a very short distance from $z = 435-580~\mu$ m, the electrons still remain in the negative-slope accelerating field at the tail of the second wake, and the negative energy chirp accumulates further as shown in Figs. 2(f) and 4(a). A local chirping strength of ~20 MeV mm⁻¹ μ m⁻¹ is estimated for the early acceleration, and its negative energy chirp increases to acquire the maximum energy spread of 3.1 MeV at t = 1.93 ps in Fig. 4(d). Subsequently, a much slower plasma down-ramp that decreases from 9 × 10¹⁸ to 6 × 10¹⁸ cm⁻³ over the acceleration stage L_{d2} is introduced to shift the *e* beam forward into the positive-slope

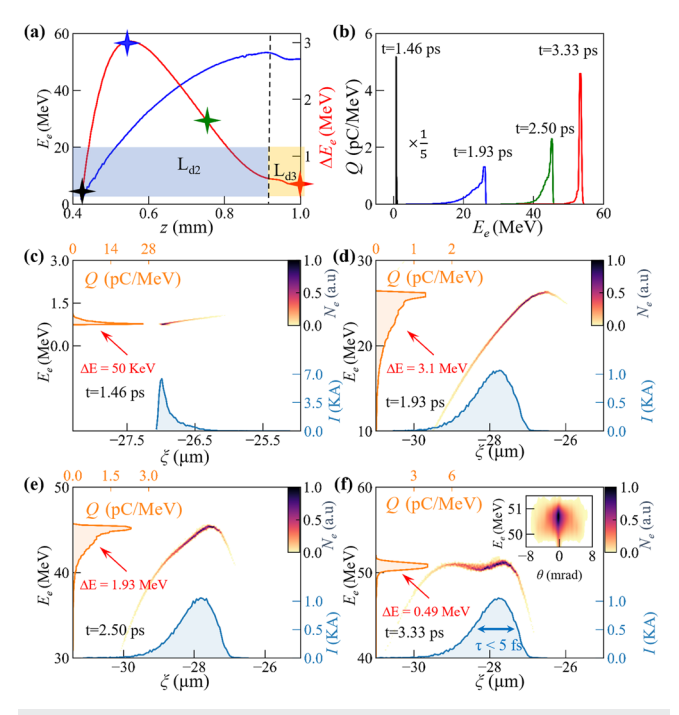


FIG. 4. (a) Evolution of energy peak value (blue curve) and energy spread (red curve) during the acceleration stage L_{d2} (blue shading) and transport stage L_{d3} (yellow shading). (b) Energy spectra for different times t=1.46 ps (black), 1.93 ps (blue), 2.50 ps (green), and 3.11 ps (red). (c)–(f) Corresponding electron phase spatial distribution, energy spectrum (orange shading), and charge current (blue shading). The inset in (f) shows the energy angular distribution of the e beam.

field zone. The accumulated negative chirp will then be mostly compensated via dechirping, before exiting the plasma at z=0.95 mm with an AES of ~0.49 MeV at t=3.33 ps, as shown in Figs. 4(e) and 4(f). In this way, the initial low AES is retained, the energy chirp can be minimized by adjusting the plasma density, and the desired energy gain can be achieved. After passing through the transport stage L_{d3} , the final output e beam with a peak energy of 51 MeV and beam charge of 4.4 pC is produced with an ultralow emittance of ~28 nm rad, energy spread of ~1%, and duration less than 5 fs. Its six-dimensional beam brightness $B_{6D,n} = I/(\varepsilon_n^2 \cdot \sigma_\delta)$ is estimated here to be as high as 2×10^{17} A/m²/0.1%, where I is the peak current, ε_n is the normalized emittance, and σ_δ is the relative energy spread in units of 0.1%.

In addition, the e-beam parameters can be tuned and controlled by adjusting the density gradient and density ratio for the down-ramp at L_{d1} . As illustrated in Figs. 5(a) and 5(c), by decreasing (or increasing) the density gradient dn_e/dz (i.e., lengthening or shortening L_{d1}) for a given density ratio n_{peak}/n_0 , the energy spread and emittance of the beam can be decreased (or increased), and a higher (or lower) energy gain can be achieved, but the beam charge decreases (or increases) accordingly under these injection conditions. The reason is that the steeper the down-ramp L_{d1} , the smaller is the phase velocity required to satisfy the conditions for fast local injection, and more electrons will be injected to increase the peak current, and a beam loading effect occurs to reduce the energy gain, leading to an increase in the emittance and energy spread as well. However, in such a weakly nonlinear plasma wake, high-brightness e beams ranging from 5 to 70 MeV with a small emittance of ≤100 nm rad and low energy spread at a few-percent level can be produced after optimization. With a larger density ratio n_{peak}/n_0 , the e-beam charge will be increased while the energy gain E_e will be decreased, as shown in Figs. 5(b) and 5(d), and a relatively large emittance of ~100 nm rad and energy spread will be introduced accordingly. However, for a steep density down-ramp L_{d1} (shown by

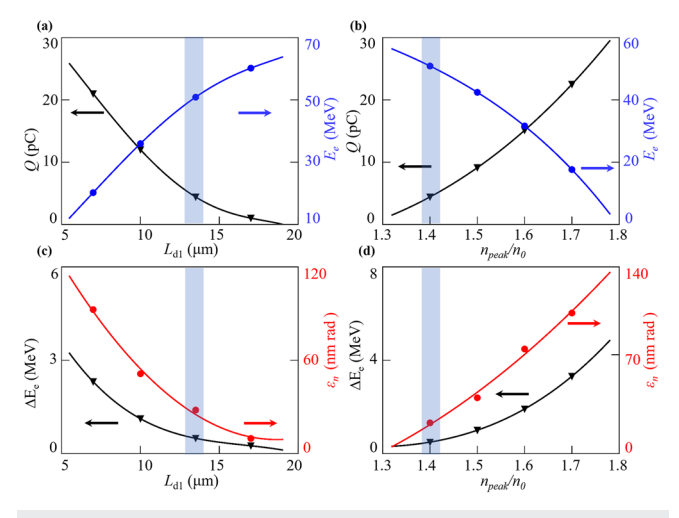


FIG. 5. (a) and (b) Charge (black curve) and energy (blue curve) as functions of the injection distance L_{d1} and the peak density $n_{\rm peak}$. (c) and (d) Corresponding energy spread (black curve) and emittance (red curve). The blue shading corresponds to the case shown in Figs. 2 and 4.

the blue shaded region), the density gradient and difference can be carefully chosen to generate an ultrahigh-brightness e beam.

In conclusion, we have proposed a simple but promising scheme to generate ultrabright e beams at around 50 MeV by exciting a weakly nonlinear laser wakefield, which, when crossing the sharp density gradient, facilitates longitudinal injection. This approach has the advantage over the bubble regime in that it produces a brighter e beam with a moderate laser driver power. Besides, longitudinal injection can also be more easily induced to obtain low-emittance e beams. By adjusting the steep density down-ramp, low-divergence electrons with initial emittance of <30 nm rad can be trapped longitudinally and then undergo chirp self-compensation during the subsequent acceleration, with the energy spread being compressed down to less than 1% when the e-beam energy reaches several tens of MeV. An ultrahigh six-dimensional beam brightness $B_{6D,n}$ of as high as 2×10^{17} A/m²/0.1% is obtained here, which is much higher than the values previously reported. It is anticipated that such bright e beams will be useful for a variety of applications, for example, as ultrafast electron probes for diffraction and imaging, in laboratory astrophysics, in coherent radiation source generation, and as high-quality electron injectors for high-energy particle acceleration.

This work was supported by the National Natural Science Foundation of China (Grant Nos. 11974251, 12105180, 12074397, 11904377, and 12005137), the Innovation Program of Shanghai Municipal Education Commission (Grant No. 2021-01-07-00-02-E00118), and the National Key Research and Development Program (Grant No. 2023YFA1406804).

AUTHOR DECLARATIONS

Conflict of Interest

The authors have no conflicts to disclose.

Author Contributions

Zhongtao Xiang: Conceptualization (equal); Data curation (equal); Investigation (equal); Visualization (equal); Writing - original draft (equal). Changhai Yu: Conceptualization (lead); Data curation (equal); Funding acquisition (equal); Investigation (equal); Methodology (equal); Supervision (equal); Validation (equal); Visualization (equal); Writing - original draft (lead); Writing - review & editing (equal). Zhiyong Qin: Conceptualization (equal); Funding acquisition (equal); Investigation (equal); Methodology (lead); Supervision (equal); Validation (equal); Visualization (equal); Writing - review & editing (equal). Xuhui Jiao: Conceptualization (equal); Funding acquisition (equal); Investigation (equal); Methodology (lead); Supervision (equal); Validation (equal); Visualization (equal); Writing - review & editing (equal). Jiahui Cheng: Investigation (equal); Validation (equal). Qiaoxuan Zhou: Investigation (equal); Validation (equal). Gatie Axi: Investigation (equal); Validation (equal). Jianghua Jie: Investigation (equal); Validation (equal). Ya Huang: Investigation (equal); Validation (equal). Jintan Cai: Investigation (equal); Validation (equal). Jiansheng Liu: Conceptualization (supporting); Funding acquisition (lead); Project administration (lead); Supervision (lead); Validation (supporting); Writing - review & editing (lead).

DATA AVAILABILITY

The data that support the findings of this study are available from the corresponding authors upon reasonable request.

REFERENCES

- ¹ J. Faure, Y. Glinec, A. Pukhov, S. Kiselev, S. Gordienko, E. Lefebvre, J. P. Rousseau, F. Burgy, and V. Malka, "A laser–plasma accelerator producing monoenergetic electron beams," Nature 431, 541–544 (2004).
- ²C. G. R. Geddes, C. Toth, J. van Tilborg, E. Esarey, C. B. Schroeder, D. Bruhwiler, C. Nieter, J. Cary, and W. P. Leemans, "High-quality electron beams from a laser wakefield accelerator using plasma-channel guiding," Nature 431, 538–541 (2004).
 ³S. P. D. Mangles, C. D. Murphy, Z. Najmudin, A. G. R. Thomas, J. L. Collier, A. E. Dangor, E. J. Divall, P. S. Foster, J. G. Gallacher, C. J. Hooker, D. A. Jaroszynski, A. J. Langley, W. B. Mori, P. A. Norreys, F. S. Tsung, R. Viskup, B. R. Walton, and K. Krushelnick, "Monoenergetic beams of relativistic electrons from intense laser-plasma interactions," Nature 431, 535–538 (2004).
- ⁴T. Tajima and J. M. Dawson, "Laser electron accelerator," Phys. Rev. Lett. 43, 267-270 (1979).
- ⁵E. Esarey, C. B. Schroeder, and W. P. Leemans, "Physics of laser-driven plasma-based electron accelerators," Rev. Mod. Phys. **81**, 1229–1285 (2009).
- ⁶A. J. Gonsalves, K. Nakamura, J. Daniels, C. Benedetti, C. Pieronek, T. C. H. de Raadt, S. Steinke, J. H. Bin, S. S. Bulanov, J. van Tilborg, C. G. R. Geddes, C. B. Schroeder, C. Toth, E. Esarey, K. Swanson, L. Fan-Chiang, G. Bagdasarov, N. Bobrova, V. Gasilov, G. Korn, P. Sasorov, and W. P. Leemans, "Petawatt laser guiding and electron beam acceleration to 8 GeV in a laser-heated capillary discharge waveguide," Phys. Rev. Lett. 122, 084801 (2019).
- ⁷C. Aniculaesei, T. Ha, S. Yoffe, L. Labun, S. Milton, E. McCary, M. M. Spinks, H. J. Quevedo, O. Z. Labun, R. Sain, A. Hannasch, R. Zgadzaj, I. Pagano, J. A. Franco-Altamirano, M. L. Ringuette, E. Gaul, S. V. Luedtke, G. Tiwari, B. Ersfeld, E. Brunetti, H. Ruhl, T. Ditmire, S. Bruce, M. E. Donovan, M. C. Downer, D. A. Jaroszynski, and B. M. Hegelich, "The acceleration of a high-charge electron bunch to 10 GeV in a 10-cm nanoparticle-assisted wakefield accelerator," Matter Radiat. Extremes 9, 014001 (2023).
- ⁸L. T. Ke, K. Feng, W. T. Wang, Z. Y. Qin, C. H. Yu, Y. Wu, Y. Chen, R. Qi, Z. J. Zhang, Y. Xu, X. J. Yang, Y. X. Leng, J. S. Liu, R. X. Li, and Z. Z. Xu, "Near-GeV electron beams at a few per-mille level from a laser wakefield accelerator via density-tailored plasma," Phys. Rev. Lett. 126, 214801 (2021).
- ⁹W. T. Wang, W. T. Li, J. S. Liu, Z. J. Zhang, R. Qi, C. H. Yu, J. Q. Liu, M. Fang, Z. Y. Qin, C. Wang, Y. Xu, F. X. Wu, Y. X. Leng, R. X. Li, and Z. Z. Xu, "High-brightness high-energy electron beams from a laser wakefield accelerator via energy chirp control," Phys. Rev. Lett. 117, 124801 (2016).
- ¹⁰Y. Glinec, J. Faure, V. Malka, T. Fuchs, H. Szymanowski, and U. Oelfke, "Radiotherapy with laser-plasma accelerators: Monte Carlo simulation of dose deposited by an experimental quasimonoenergetic electron beam," Med. Phys. 33, 155–162 (2006).
- ¹¹V. Malka, J. Faure, Y. A. Gauduel, E. Lefebvre, A. Rousse, and K. T. Phuoc, "Principles and applications of compact laser-plasma accelerators," Nat. Phys. 4, 447–453 (2008).
- ¹²B. Kettle, E. Gerstmayr, M. J. V. Streeter, F. Albert, R. A. Baggott, N. Bourgeois, J. M. Cole, S. Dann, K. Falk, I. Gallardo Gonzalez, A. E. Hussein, N. Lemos, N. C. Lopes, O. Lundh, Y. Ma, S. J. Rose, C. Spindloe, D. R. Symes, M. Smid, A. G. R. Thomas, R. Watt, and S. P. D. Mangles, "Single-shot multi-keV X-ray absorption spectroscopy using an ultrashort laser-wakefield accelerator source," Phys. Rev. Lett. 123, 254801 (2019).
- ¹³B. Mahieu, N. Jourdain, K. Ta Phuoc, F. Dorchies, J. P. Goddet, A. Lifschitz, P. Renaudin, and L. Lecherbourg, "Probing warm dense matter using femtosecond X-ray absorption spectroscopy with a laser-produced betatron source," Nat. Commun. 9, 3276 (2018).
- ¹⁴W. Wang, K. Feng, L. Ke, C. Yu, Y. Xu, R. Qi, Y. Chen, Z. Qin, Z. Zhang, M. Fang, J. Liu, K. Jiang, H. Wang, C. Wang, X. Yang, F. Wu, Y. Leng, J. Liu, R. Li, and Z. Xu, "Free-electron lasing at 27 nanometres based on a laser wakefield accelerator," Nature 595, 516–520 (2021).
- ¹⁵M. Labat, J. C. Cabadağ, A. Ghaith, A. Irman, A. Berlioux, P. Berteaud, F. Blache, S. Bock, F. Bouvet, F. Briquez, Y.-Y. Chang, S. Corde, A. Debus, C. De

- Oliveira, J.-P. Duval, Y. Dietrich, M. El Ajjouri, C. Eisenmann, J. Gautier, R. Gebhardt, S. Grams, U. Helbig, C. Herbeaux, N. Hubert, C. Kitegi, O. Kononenko, M. Kuntzsch, M. LaBerge, S. Lê, B. Leluan, A. Loulergue, V. Malka, F. Marteau, M. H. N. Guyen, D. Oumbarek-Espinos, R. Pausch, D. Pereira, T. Püschel, J.-P. Ricaud, P. Rommeluere, E. Roussel, P. Rousseau, S. Schöbel, M. Sebdaoui, K. Steiniger, K. Tavakoli, C. Thaury, P. Ufer, M. Valléau, M. Vandenberghe, J. Vétéran, U. Schramm, and M.-E. Couprie, "Seeded free-electron laser driven by a compact laser plasma accelerator," Nat. Photonics 17, 150–156 (2022).
- ¹⁶ K. Ta Phuoc, S. Corde, C. Thaury, V. Malka, A. Tafzi, J. P. Goddet, R. C. Shah, S. Sebban, and A. Rousse, "All-optical Compton gamma-ray source," Nat. Photonics 6, 308–311 (2012).
- ¹⁷G. Sarri, D. J. Corvan, W. Schumaker, J. M. Cole, A. Di Piazza, H. Ahmed, C. Harvey, C. H. Keitel, K. Krushelnick, S. P. Mangles, Z. Najmudin, D. Symes, A. G. Thomas, M. Yeung, Z. Zhao, and M. Zepf, "Ultrahigh brilliance multi-MeV γ-ray beams from nonlinear relativistic Thomson scattering," Phys. Rev. Lett. 113, 224801 (2014)
- ¹⁸C. Yu, R. Qi, W. Wang, J. Liu, W. Li, C. Wang, Z. Zhang, J. Liu, Z. Qin, M. Fang, K. Feng, Y. Wu, Y. Tian, Y. Xu, F. Wu, Y. Leng, X. Weng, J. Wang, F. Wei, Y. Yi, Z. Song, R. Li, and Z. Xu, "Ultrahigh brilliance quasi-monochromatic MeV γ-rays based on self-synchronized all-optical Compton scattering," Sci. Rep. 6, 29518 (2016).
- ¹⁹N. A. Mikheytsev and A. V. Korzhimanov, "Generation of synchronized x-rays and mid-infrared pulses by Doppler-shifting of relativistically intense radiation from near-critical-density plasmas," Matter Radiat. Extremes **8**, 024401 (2023).
- ²⁰Y. Zhao, H. Lu, C. Zhou, and J. Zhu, "Overcritical electron acceleration and betatron radiation in the bubble-like structure formed by re-injected electrons in a tailored transverse plasma," Matter Radiat. Extremes 8, 014403 (2023).
- ²¹ C. Yu, J. Liu, W. Wang, W. Li, R. Qi, Z. Zhang, Z. Qin, J. Liu, M. Fang, K. Feng, Y. Wu, L. Ke, Y. Chen, C. Wang, Y. Xu, Y. Leng, C. Xia, R. Li, and Z. Xu, "Enhanced betatron radiation by steering a laser-driven plasma wakefield with a tilted shock front," Appl. Phys. Lett. 112, 133503 (2018).
- ²² M. Kozlova, I. Andriyash, J. Gautier, S. Sebban, S. Smartsev, N. Jourdain, U. Chaulagain, Y. Azamoum, A. Tafzi, J.-P. Goddet, K. Oubrerie, C. Thaury, A. Rousse, and K. Ta Phuoc, "Hard X rays from laser-wakefield accelerators in density tailored plasmas," Phys. Rev. X 10, 011061 (2020).
- ²³R. Rakowski, P. Zhang, K. Jensen, B. Kettle, T. Kawamoto, S. Banerjee, C. Fruhling, G. Golovin, D. Haden, M. S. Robinson, D. Umstadter, B. A. Shadwick, and M. Fuchs, "Transverse oscillating bubble enhanced laser-driven betatron X-ray radiation generation," Sci. Rep. 12, 10855 (2022).
- ²⁴Z. H. He, B. Hou, J. A. Nees, J. H. Easter, J. Faure, K. Krushelnick, and A. G. R. Thomas, "High repetition-rate wakefield electron source generated by few-millipoule, 30 fs laser pulses on a density downramp," New J. Phys. 15, 053016 (2013).
- ²⁵D. Guénot, D. Gustas, A. Vernier, B. Beaurepaire, F. Böhle, M. Bocoum, M. Lozano, A. Jullien, R. Lopez-Martens, A. Lifschitz, and J. Faure, "Relativistic electron beams driven by kHz single-cycle light pulses," Nat. Photonics 11, 293–296 (2017)
- ²⁶F. Salehi, A. J. Goers, G. A. Hine, L. Feder, D. Kuk, B. Miao, D. Woodbury, K. Y. Kim, and H. M. Milchberg, "MeV electron acceleration at 1 kHz with <10 mJ laser pulses," Opt. Lett. 42, 215–218 (2017).</p>
- ²⁷C. Lazzarini, G. Grittani, P. Valenta, I. Zymak, R. Antipenkov, U. Chaulagain, L. Goncalves, A. Grenfell, M. Lamac, and S. Lorenz, "50 MeV electron beams accelerated by a terawatt scalable kHz laser," arXiv:2302.11415 (2023).
- ²⁸ A. J. Goers, G. A. Hine, L. Feder, B. Miao, F. Salehi, J. K. Wahlstrand, and H. M. Milchberg, "Multi-MeV electron acceleration by subterawatt laser pulses," Phys. Rev. Lett. 115, 194802 (2015).
- ²⁹ A. Benedetti, M. Tamburini, and C. H. Keitel, "Giant collimated gamma-ray flashes," Nat. Photonics 12, 319–323 (2018).
- ³⁰M. Yamada, L. J. Chen, J. Yoo, S. Wang, W. Fox, J. Jara-Almonte, H. Ji, W. Daughton, A. Le, J. Burch, B. Giles, M. Hesse, T. Moore, and R. Torbert, "The two-fluid dynamics and energetics of the asymmetric magnetic reconnection in laboratory and space plasmas," Nat. Commun. **9**, 5223 (2018).

- ³¹ A. F. Lifschitz and V. Malka, "Optical phase effects in electron wake-field acceleration using few-cycle laser pulses," New J. Phys. 14, 053045 (2012).
- ³²B. Beaurepaire, A. Lifschitz, and J. Faure, "Electron acceleration in subrelativistic wakefields driven by few-cycle laser pulses," New J. Phys. 16, 023023 (2014).
- ³³D. Gustas, D. Guénot, A. Vernier, S. Dutt, F. Böhle, R. Lopez-Martens, A. Lifschitz, and J. Faure, "High-charge relativistic electron bunches from a kHz laser-plasma accelerator," Phys. Rev. Accel. Beams 21, 013401 (2018).
- ³⁴F. Salehi, M. Le, L. Railing, M. Kolesik, and H. M. Milchberg, "Laser-accelerated, low-divergence 15-MeV quasimonoenergetic electron bunches at 1 kHz," Phys. Rev. X 11, 021055 (2020).
- ³⁵L. Rovige, J. Huijts, I. Andriyash, A. Vernier, V. Tomkus, V. Girdauskas, G. Raciukaitis, J. Dudutis, V. Stankevic, P. Gecys, M. Ouille, Z. Cheng, R. Lopez-Martens, and J. Faure, "Demonstration of stable long-term operation of a kilohertz laser-plasma accelerator," Phys. Rev. Accel. Beams 23, 093401 (2020).
- ³⁶S. Corde, C. Thaury, A. Lifschitz, G. Lambert, K. Ta Phuoc, X. Davoine, R. Lehe, D. Douillet, A. Rousse, and V. Malka, "Observation of longitudinal and transverse self-injections in laser-plasma accelerators," Nat. Commun. 4, 1501 (2013).
- ³⁷Z.-H. He, A. G. R. Thomas, B. Beaurepaire, J. A. Nees, B. Hou, V. Malka, K. Krushelnick, and J. Faure, "Electron diffraction using ultrafast electron bunches from a laser-wakefield accelerator at kHz repetition rate," Appl. Phys. Lett. 102, 064104 (2013).
- ³⁸J. Faure, B. van der Geer, B. Beaurepaire, G. Gallé, A. Vernier, and A. Lifschitz, "Concept of a laser-plasma-based electron source for sub-10-fs electron diffraction," Phys. Rev. Accel. Beams 19, 021302 (2016).
- ³⁹ H. P. Schlenvoigt, K. Haupt, A. Debus, F. Budde, O. Jäckel, S. Pfotenhauer, H. Schwoerer, E. Rohwer, J. G. Gallacher, E. Brunetti, R. P. Shanks, S. M. Wiggins, and D. A. Jaroszynski, "A compact synchrotron radiation source driven by a laser-plasma wakefield accelerator," Nat. Phys. 4, 130–133 (2007).
- ⁴⁰ M. Fuchs, R. Weingartner, A. Popp, Z. Major, S. Becker, J. Osterhoff, I. Cortrie, B. Zeitler, R. Hörlein, G. D. Tsakiris, U. Schramm, T. P. Rowlands-Rees, S. M. Hooker, D. Habs, F. Krausz, S. Karsch, and F. Grüner, "Laser-driven soft-X-ray undulator source," Nat. Phys. 5, 826–829 (2009).
- ⁴¹S. Corde, K. Ta Phuoc, G. Lambert, R. Fitour, V. Malka, A. Rousse, A. Beck, and E. Lefebvre, "Femtosecond x rays from laser-plasma accelerators," Rev. Mod. Phys. **85**, 1–48 (2013).
- ⁴²E. Adli, A. Ahuja, O. Apsimon, R. Apsimon, A. M. Bachmann, D. Barrientos, F. Batsch, J. Bauche, V. K. Berglyd Olsen, M. Bernardini, T. Bohl, C. Bracco, F. Braunmuller, G. Burt, B. Buttenschon, A. Caldwell, M. Cascella, J. Chappell, E. Chevallay, M. Chung, D. Cooke, H. Damerau, L. Deacon, L. H. Deubner, A. Dexter, S. Doebert, J. Farmer, V. N. Fedosseev, R. Fiorito, R. A. Fonseca, F. Friebel, L. Garolfi, S. Gessner, I. Gorgisyan, A. A. Gorn, E. Granados, O. Grulke, E. Gschwendtner, J. Hansen, A. Helm, J. R. Henderson, M. Huther, M. Ibison, L. Jensen, S. Jolly, F. Keeble, S. Y. Kim, F. Kraus, Y. Li, S. Liu, N. Lopes, K. V. Lotov, L. Maricalva Brun, M. Martyanov, S. Mazzoni, D. Medina Godoy, V. A. Minakov, J. Mitchell, J. C. Molendijk, J. T. Moody, M. Moreira, P. Muggli, E. Oz, C. Pasquino, A. Pardons, F. Pena Asmus, K. Pepitone, A. Perera, A. Petrenko, S. Pitman, A. Pukhov, S. Rey, K. Rieger, H. Ruhl, J. S. Schmidt, I. A. Shalimova, P. Sherwood, L. O. Silva, L. Soby, A. P. Sosedkin, R. Speroni, R. I. Spitsyn, P. V. Tuev, M. Turner, F. Velotti, L. Verra, V. A. Verzilov, J. Vieira, C. P. Welsch, B. Williamson, M. Wing, B. Woolley, and G. Xia, "Acceleration of electrons in the plasma wakefield of a proton bunch," Nature 561, 363-367 (2018).
- ⁴³A. Buck, J. Wenz, J. Xu, K. Khrennikov, K. Schmid, M. Heigoldt, J. M. Mikhailova, M. Geissler, B. Shen, F. Krausz, S. Karsch, and L. Veisz, "Shock-front injector for high-quality laser-plasma acceleration," Phys. Rev. Lett. **110**, 185006 (2013).
- ⁴⁴J. Faure, C. Rechatin, O. Lundh, L. Ammoura, and V. Malka, "Injection and acceleration of quasimonoenergetic relativistic electron beams using density gradients at the edges of a plasma channel," Phys. Plasmas 17, 083107 (2010).
- ⁴⁵L. T. Ke, C. h. Yu, K. Feng, Z. Y. Qin, K. N. Jiang, H. Wang, S. X. Luan, X. J. Yang, Y. Xu, Y. X. Leng, W. T. Wang, J. S. Liu, and R. X. Li, "Optimization of

- electron beams based on plasma-density modulation in a laser-driven wakefield accelerator," Appl. Sci. 11, 2560 (2021).
- ⁴⁶C. S. Hue, Y. Wan, E. Y. Levine, and V. Malka, "Control of electron beam current, charge, and energy spread using density downramp injection in laser wakefield accelerators," Matter Radiat. Extremes **8**, 024401 (2023).
- ⁴⁷G. Fubiani, E. Esarey, C. B. Schroeder, and W. P. Leemans, "Improvement of electron beam quality in optical injection schemes using negative plasma density gradients," Phys. Rev. E **73**, 026402 (2006).
- ⁴⁸R. Lehe, M. Kirchen, I. A. Andriyash, B. B. Godfrey, and J.-L. Vay, "A spectral, quasi-cylindrical and dispersion-free Particle-In-Cell algorithm," Comput. Phys. Commun. 203, 66–82 (2016).
- ⁴⁹N. Bourgeois, J. Cowley, and S. M. Hooker, "Two-pulse ionization injection into quasilinear laser wakefields," Phys. Rev. Lett. **111**, 155004 (2013).
- ⁵⁰E. Esarey and M. Pilloff, "Trapping and acceleration in nonlinear plasma waves," Phys. Plasmas 2, 1432–1436 (1995).